Periodic chain clusters of two-dimensional bubbles

2002 J. Phys.: Condens. Matter 14 5719

(http://iopscience.iop.org/0953-8984/14/23/306)

INSTITUTE OF PHYSICS PUBLISHING JOURNAL OF PHYSICS: CONDENSED MATTER

J. Phys.: Condens. Matter **14** (2002) 5719–5730 PII: S0953-8984(02)33556-2

Periodic chain clusters of two-dimensional bubbles

P I C Teixeira[1,2] **and M A Fortes**[2]

[1] Faculdade de Engenharia, Universidade Católica Portuguesa, Estrada de Talaíde, P-2635-631 Rio de Mouro, Portugal
[2] Departamento de Engenharia de Materiais, e Instituto de Ciência e Engenharia de Materiais e Superfícies, Instituto Superior Técnico, Avenida Rovisco Pais, P-1049-001 Lisbon, Portugal

Received 6 February 2002, in final form 25 March 2002
Published 30 May 2002
Online at stacks.iop.org/JPhysCM/14/5719

Abstract

We study periodic chain clusters comprising equal numbers of two-dimensional bubbles of two different areas, with at most four bubbles per period. The cluster energies are calculated as a function of the ratio λ of bubble areas and of the imposed strain ϵ. We identify the clusters of lowest energy for each (λ, ϵ), and obtain the Young's moduli of all clusters in their unstrained state. An approximately linear correlation has been found between the Young's moduli and the cluster binding energy per unit area, similar to that which holds for crystalline solids (e.g. metals).

1. Introduction

Bubble clusters—foams—have attracted considerable attention, particularly because they are paradigms for a variety of cellular structures, from polycrystals to biological tissues. Two main types of bubble cluster have been discussed in the literature: finite, and unbounded periodic. Most studies have dealt with two-dimensional clusters, which are easier to analyse and study experimentally. The main problems addressed have been (a) ageing [1, 2], (b) deformation [3] and (c) the calculation of cluster energies [4–6], particularly with a view to identifying the lowest-energy cluster for a given composition (i.e. for given numbers and sizes of the assembled bubbles). This requires solving clusters for their equilibrium configurations: once their topology (specified by the number and sequence of bubble contacts) and bubble areas (assuming incompressibility) have been fixed, their geometry still needs to be found [7]. Different geometries correspond to different strain (stress) states; note that there may not be a solution for certain area ratios, see below.

The necessary conditions for the equilibrium of a cluster are known as Plateau's laws [8]. They relate to the balance of pressures and film tensions, leading to films of constant mean curvature meeting three at a time at 120° angles. These conditions, together with the sizes of individual bubbles, give as many equations as there are independent variables [7]. However, as recenlty shown by Weaire *et al* [9], this does not necessarily imply a unique solution (i.e., geometry) for the cluster. For unbounded clusters, on the other hand, the number of variables

exceeds the number of equations [7], and there is a whole range of strained configurations that satisfy Plateau's laws, for given topology and bubble areas.

Clusters are usually assumed to be 'dry', with negligible Plateau borders, and containing an incompressible gas of constant energy. The free energy E of a cluster is then just its surface free energy,

$$E = \gamma P, \tag{1}$$

where P is the total area (length) of films.

Finite clusters are embedded in an atmosphere at pressure p_0. At equilibrium, each bubble i of size S_i (volume or area) has an internal pressure p_i. The following relation then holds for a finite free cluster [4, 10]:

$$E = \frac{d}{d-1} \sum_i S_i (p_i - p_0), \tag{2}$$

where $d = 2$ or 3 is the dimensionality of the cluster. Periodic unbounded clusters are defined by a unit cell—the repeating unit—containing N bubbles. For such clusters there is no 'outside', hence no p_0, and equation (2) no longer applies.

In this paper we discuss a third category of two-dimensional bubble clusters, which we name *chain clusters*, consisting of periodic strings of bubbles with N-bubble unit cells. Such chain clusters are unbounded (and periodic) in one direction, but finite in the transverse direction; they are immersed in the foam gas at pressure p_0 (see figure 1 for some examples). As shown elsewhere [7], the Plateau rules do not completely determine the geometry of a chain cluster of given topology and bubble sizes: as for unbounded two-dimensional periodic clusters, it is necessary to specify the strain, which in this case is a single scalar quantity. For every chain cluster that we have considered, there is only one unstrained (or free) configuration for which the energy reaches a minimum. Our analysis concentrates on calculating the energy as a function of the imposed strain for each possible topology; from this we extract the unstrained geometries (i.e. those corresponding to the minima of the energy) and the Young's moduli.

Chain clusters mimic long linear molecules where the cohesion between 'atoms' (i.e. bubbles) is due to the decrease in surface energy when they come together to form the 'molecule' (i.e. the foam cluster). Because they are easier to analyse than periodic two-dimensional clusters, they allow us more readily to identify issues to explore in higher dimensions.

2. Chain clusters under consideration

We discuss two-dimensional chain clusters containing equal numbers of bubbles of two different areas, A_1 and A_2, each bubble being composed of at least two films. Only those clusters are considered in which all bubbles of a given area have the same topology, i.e. the same neighbours, and also the same (internal) pressure. In particular, adjacent bubbles of the same area are separated by a straight boundary at equilibrium. This requirement implies that our chain clusters have at most four bubbles per unit cell[3], i.e. $N = 4$. Even with these restrictions, we have been able to draw 22 possible topologies, shown schematically in figure 2.

Chain clusters of this type fall into one of two main classes: those with (figures 2(a), (c)) and those without (figures 2(b), (d)) bubbles that go across the cluster, i.e. that contact the outside gas on either side of the chain. Each of these classes in turn divides into two subclasses, depending on whether the cluster contains 'inner' bubbles (i.e. those that do not

[3] Readers can easily convince themselves by constructing, for example, cluster $4_3 4_3$. Re-draw cluster $4_2 4_2$ in figure 1(b) with six bubbles per unit cell: clearly all bubbles of size, say, A_1 are no longer equivalent, as the 'middle' bubble borders on two other bubbles of size A_1, whereas each of the latter borders on one bubble of size A_1 and one of size A_2. Likewise for bubbles of size A_2.

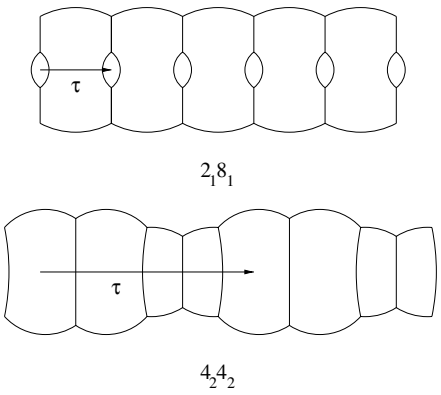

Figure 1. Chain clusters of types $2_1 8_1$ and $4_2 4_2$ (see the text and figure 2 for notation). The films are arcs of circle meeting at 120° angles at the vertices. $\boldsymbol{\tau}$ is the period.

contact the outside) or not. Conventionally, we take $A_1 = 1$ as the area of the bubble with more films, and set the area of the other bubble $A_2 = \lambda$. A simple notation is introduced for clusters which tells how many films there are per bubble and how many bubbles of each area there are per unit cell. Thus for example $4_1 4_1$ means 'one four-sided bubble of area λ plus one four-sided bubble of area 1 per unit cell'. Likewise, $3_2 7_2$ means 'two three-sided bubbles of area λ plus two seven-sided bubbles of area 1 per unit cell'. In a few cases, for example $3_2 6_2$, there is more than one topology consistent with a given number of films per bubble and a given number of bubbles of each area per cell; these we distinguish by the additional subscript A, B and C, as appropriate. Note that clusters $4_1 4_1$ and $5_1 5_1$ are unique in that all their bubbles have the same topology; for $\lambda = 1$, they consist of identical bubbles.

If $\boldsymbol{\tau}$ is the symmetry translation vector along the chain cluster, we define $\boldsymbol{t} = \boldsymbol{\tau}/n$, where $n = N/2 = 1$ or 2 is the number of pairs of bubbles per period; $t \equiv |\boldsymbol{t}|$ is thus the length along the cluster axis per pair of bubbles. For each of the clusters under consideration we write down the equations that express Plateau's laws, and those for the areas of the bubbles, in terms of the lengths of films and the angles at which they meet (see the appendix for details). The number of variables exceeds the number of equations by one [7] (clusters containing two-sided bubbles—for example, $2_2 8_2$—or pairs of adjacent three-sided bubbles have trivial extra variables specifying their location on the edges they 'decorate', which do not enter the expression for the energy). We take t as the free, or independent, variable: it defines the strain $\epsilon \equiv \log(t/t^*)$, where t^* corresponds to a cluster with no applied forces, and therefore minimum energy. For $t < t^*$ the cluster is compressed, while for $t > t^*$ it is stretched.

Most clusters exhibit some symmetries (e.g., with respect to the chain axis), which simplifies calculations. In general, a cluster of given topology may exist only in certain ranges of t and λ, at the ends of which the lengths of one or more of its films vanish. We call the cluster that has lowest energy in a region of (λ, t) space the *minimal* cluster in that region. All clusters are assumed to be stable in the ranges of λ where they are realizable; this is confirmed *a posteriori* by the fact that their perimeters are convex functions of t for all λ investigated.

3. Young's modulus of chain clusters

It is interesting to compare the stiffnesses—i.e. the Young's moduli—along $\boldsymbol{t}$ of the various chain clusters. Start by introducing an average cross-sectional width of the cluster w, given by

$$w = \frac{A_1 + A_2}{2t} = \frac{1 + \lambda}{2t}. \tag{3}$$

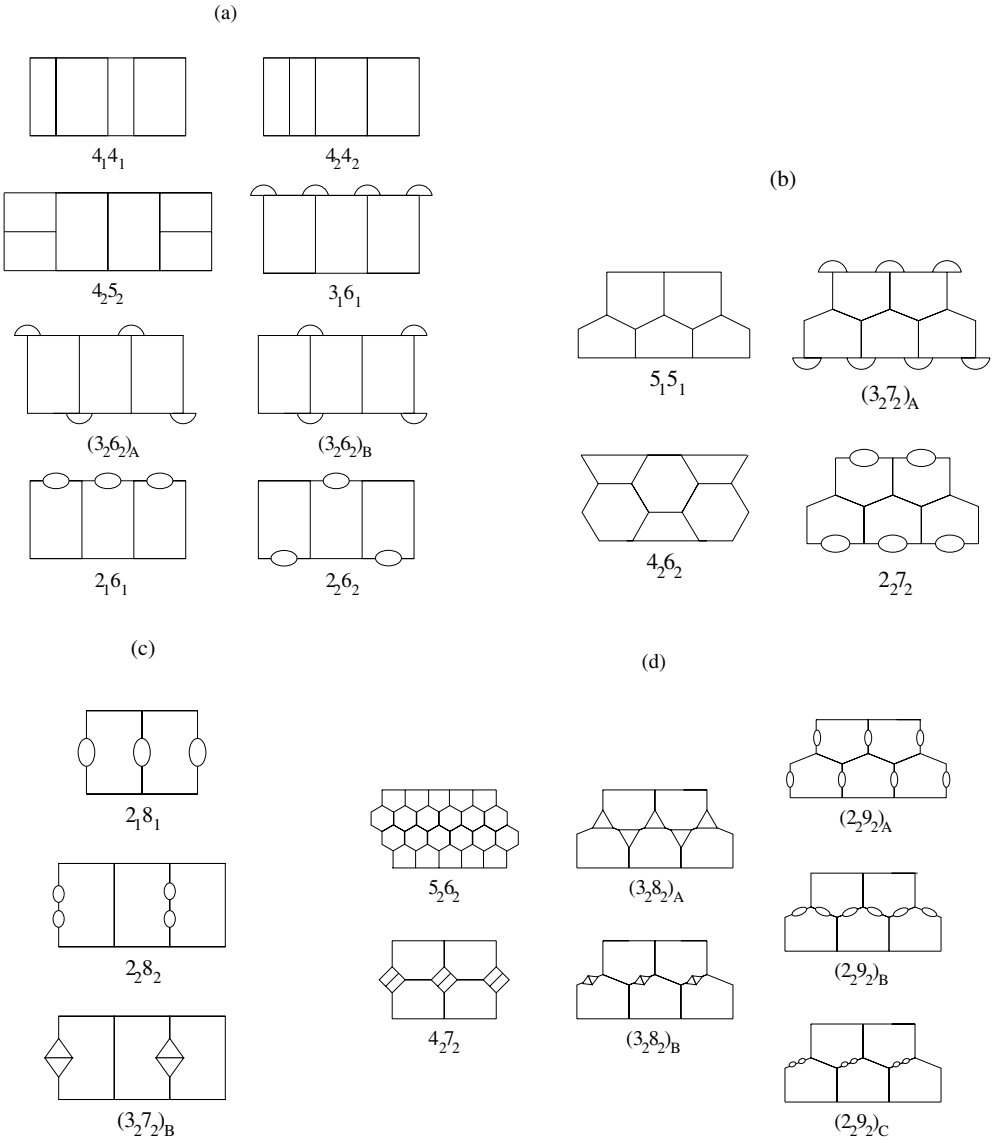

Figure 2. The 22 chain clusters with bubbles of areas 1 and λ in one-to-one proportion and at most four bubbles per period. They divide into four classes, depending on whether they contain (*a*) bubbles that span the cluster width but no inner bubbles, (*b*) neither bubbles that span the cluster width nor inner bubbles, (*c*) bubbles that span the cluster width and inner bubbles or (*d*) inner bubbles but no bubbles that span the cluster width (see the text for details). In this schematic representation only the topologies (i.e. the bubble connectivities) are rendered accurately: in the actual clusters, all films are arcs of circle meeting at 120° angles at the vertices (see figure 1). Note that clusters $2_1 6_1$ and $2_2 6_2$ have the same perimeter.

The strain increment along the chain is $\mathrm{d}\epsilon = \mathrm{d}t/t$, which is achieved by applying force F per pair of bubbles, along the axis of the cluster, with

$$F = -\frac{\mathrm{d}E}{\mathrm{d}t}. \tag{4}$$

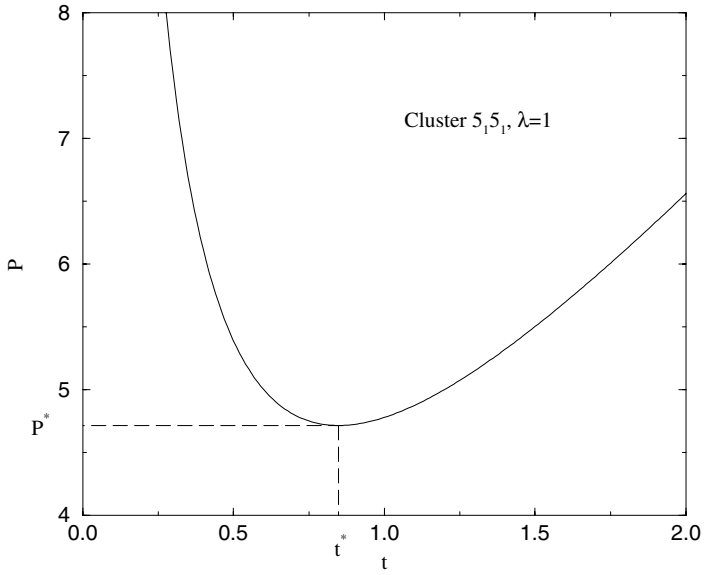

Figure 3. $P(t)$, the perimeter per pair of bubbles as a function of strain, for cluster $5_1 5_1$ of figure 2 with $\lambda = 1$: the minimum perimeter P^* is attained at $t = t^*$.

Note that equation (2) is only valid when $F = 0$; if $F \neq 0$ ($t \neq t^*$), it has to be modified to include a strain energy term. We define Young's modulus as

$$Y = \frac{\mathrm{d}F}{\mathrm{d}w} = -\frac{1}{w}\frac{\mathrm{d}F}{\mathrm{d}\epsilon} = -\frac{t}{w}\frac{\mathrm{d}F}{\mathrm{d}t}. \tag{5}$$

Simple manipulations lead to

$$\frac{Y}{\gamma} = \frac{2t^2}{1+\lambda}\frac{\mathrm{d}^2 P}{\mathrm{d}t^2}. \tag{6}$$

We have calculated the Young's moduli at the minima of the $P(\lambda, t)$ curves, $Y^* \equiv Y(\lambda, t^*)$. In these cases Y^* is the maximum of $Y(\lambda, t)$ at fixed λ.

4. Results and discussion

We performed calculations for $0.1 \leqslant \lambda \leqslant 8$ and $0.01 \leqslant t \leqslant 5$. Figure 3 shows a typical $P(t)$ curve ($\equiv P(\lambda, t)$ at fixed λ), for cluster $5_1 5_1$ of figure 2. The perimeter $P(t)$ has a minimum, P^*, at $t = t^*$. From equation (6), the Young's modulus Y^* is proportional to the curvature of $P(t)$ at the minimum. In figure 4 we plot, for $\lambda = 0.125$, $P(t)$ for all *minimal clusters*—clusters that have the least perimeter in some range of t ($0.01 \leqslant t \leqslant 5$). The transitions between minimal clusters can be either 'continuous' (if the corresponding $P(t)$ curves cross) or 'discontinuous' (if there is a jump between curves). For illustration purposes we have also included in figure 4 cluster $2_2 8_2$, which is never minimal; the curves for this and all other non-minimal clusters obviously lie above those for the minimal clusters. Similar pictures are obtained for the other values of λ investigated ($0.1 \leqslant \lambda \leqslant 8$). Note that clusters may 'lose' their minima as λ is varied (i.e. such minima may occur at values of t for which one or more of the films have zero or negative lengths), but remain stable throughout (in the sense that $P(t)$ is always convex).

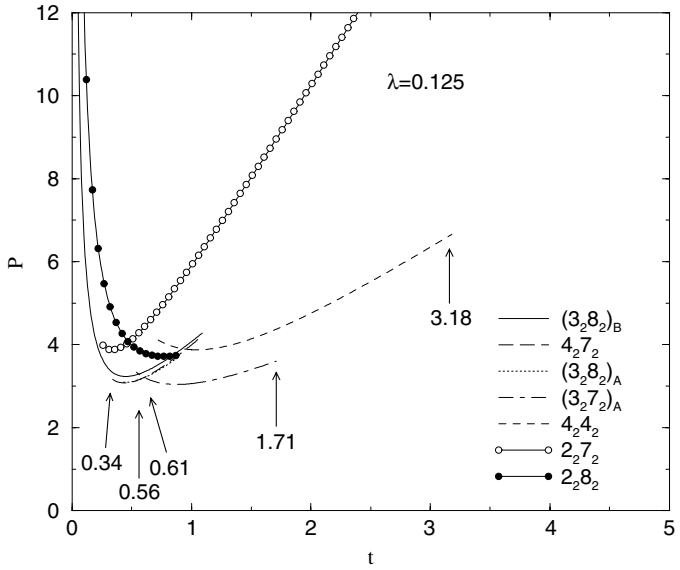

Figure 4. $P(t)$ for all clusters that are minimal in some range of t for $\lambda = 0.125$. The curve for the non-minimal cluster 2_28_2 is included for illustration purposes. Transitions between different minimal clusters are marked with arrows and the corresponding values of t: these can be either continuous, when two curves cross, or discontinuous, when there is a jump from one curve to the other.

The 'phase diagram' of figure 5 summarizes which cluster is minimal in which region(s) of the (λ, t) plane, for $0.01 \leqslant t \leqslant 5$ and $0.1 \leqslant \lambda \leqslant 8$. There are a total of nine minimal clusters, with one of them, $(3_26_2)_B$, covering a rather small area. It is also noteworthy that clusters 5_15_1 and 4_26_2 are re-entrant, in the sense that for some λ they are each minimal in two disjoint ranges of t. Cluster 4_24_2 is minimal in a larger region than any other, mostly at intermediate to large t; if λ is small, however, the minimal cluster at larger t is 2_27_2. Still, it is important to bear in mind that some, or all, of these features may change for λ beyond the range that we have explored.

How P^* and Y^* vary as a function of λ can be seen in figures 6 and 7, respectively. Recall that any cluster may exist only in a certain range of λ, at the ends of which the lengths of one or more of its films go to zero. As expected, P^* increases with increasing λ, while Y^* decreases—i.e. all clusters go 'softer' as the bubbles with fewer sides grow bigger.

We have attempted to correlate Y^*/γ with the binding energy per unit area, defined as

$$\frac{E_b}{\gamma} = \frac{2\sqrt{\pi}(1+\sqrt{\lambda}) - P^*}{1+\lambda}, \tag{7}$$

where the first term is the energy of separate (circular) bubbles of areas 1 and λ. In figure 8(a) we plot Y^*/γ versus E_b/γ, using the data from figures 6 and 7: there is an approximately linear correlation. Strikingly, a very similar result is obtained for metals ($Y \sim 2.55E_b$, see figure 8(b)) [11], which is due to the fact that the position of the minimum of the interatomic potential (i.e. the atomic radius) varies little across the periodic table. We therefore speculate that the same correlation in chain clusters follows from the likewise small spread of t^*, the position of the minimum of $P(t)$ (as figure 4 illustrates).

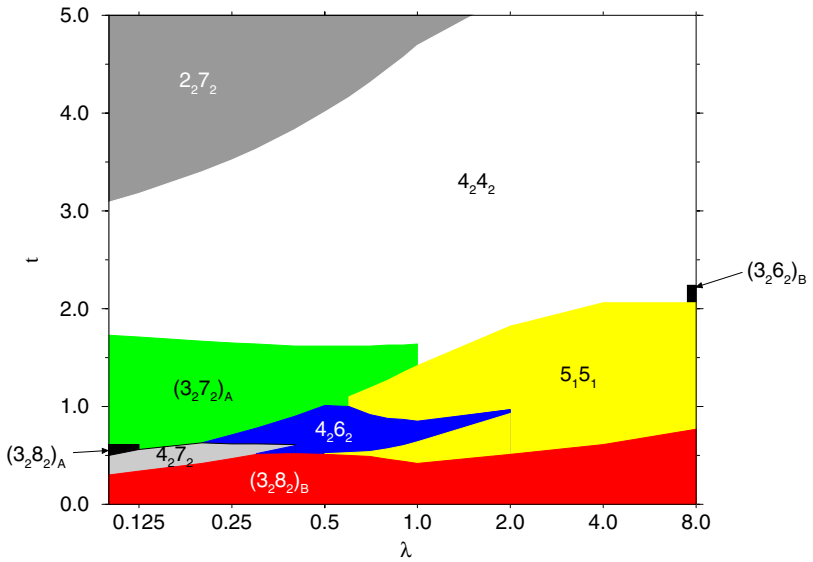

Figure 5. 'Phase diagram' of chain clusters in the (λ, t) plane, showing where each of them is minimal for $0.01 \leqslant t \leqslant 5$ and $0.1 \leqslant \lambda \leqslant 8$ (note the logarithmic scale along the horizontal axis). The width (i.e. λ-extent) of the $(3_26_2)_B$ region has been exaggerated for clarity. Recall that t is the length along the cluster axis *per pair* of bubbles.

(This figure is in colour only in the electronic version)

5. Summary

We have calculated the geometries of periodic chain clusters of all possible topologies compatible with a unit cell containing no more than four bubbles of two different areas, as a function of the area ratio and applied strain. The energies and Young's moduli of the clusters have also been computed. The Young's modulus was shown to correlate nearly linearly with the cluster binding energy per unit area. This type of analysis can, in principle, be extended—at a price—to two-dimensional clusters with *two* directions of periodicity. Further extension to three-dimensional periodic clusters, including three-dimensional chain clusters, would be even harder, probably requiring Surface Evolver [12] calculations.

Acknowledgments

PICT acknowledges funding from the Fundação para a Ciência e Tecnologia (Portugal). We are grateful to Professor A Pádua Loureiro for helpful discussions, and would like to thank one of the anonymous referees for spotting a mistake in the original manuscript.

Appendix. Chain cluster calculations

A two-dimensional chain cluster of a given topology is solved as follows. First we define a cluster skeleton by connecting the vertices of the cluster by straight-line segments. We thus obtain a network with the topology (connectivity) of the cluster. The lengths of these segments are denoted L_i, and the angles between segments (i and k, say) at triple points by α_{ik}. The L_i and α_{ik} are of course not independent, and we can choose either as the free variables when

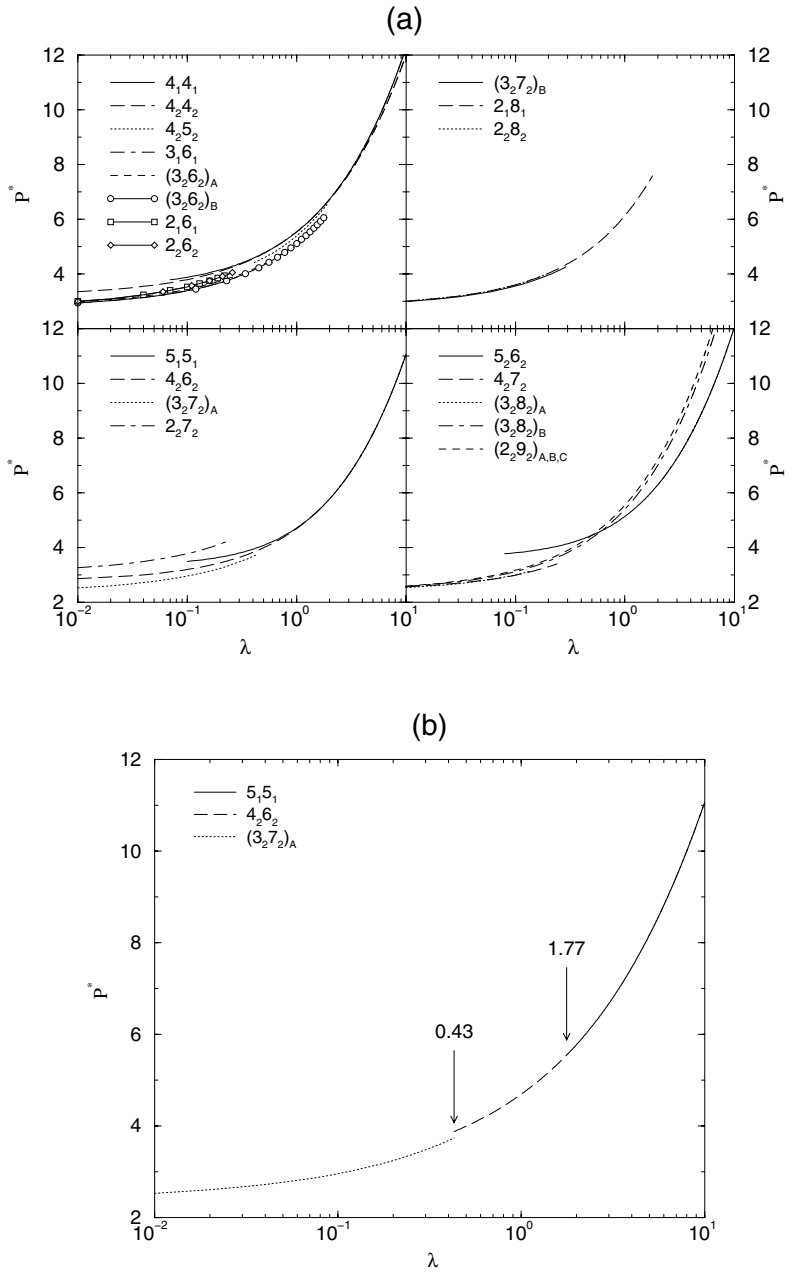

Figure 6. (*a*) P^* versus λ for all clusters, grouped as in figure 2. (*b*) Smallest P^* ('minimal', or unstrained, clusters) in each range of λ. Note the log-lin scale.

introducing the equations that relate them. Next, we associate with each line segment a radius R_i and a subtended angle $2\theta_i$ of the film (see figure 9), with an appropriate sign convention. We have

$$L_i = 2R_i \sin\theta_i. \tag{A.1}$$

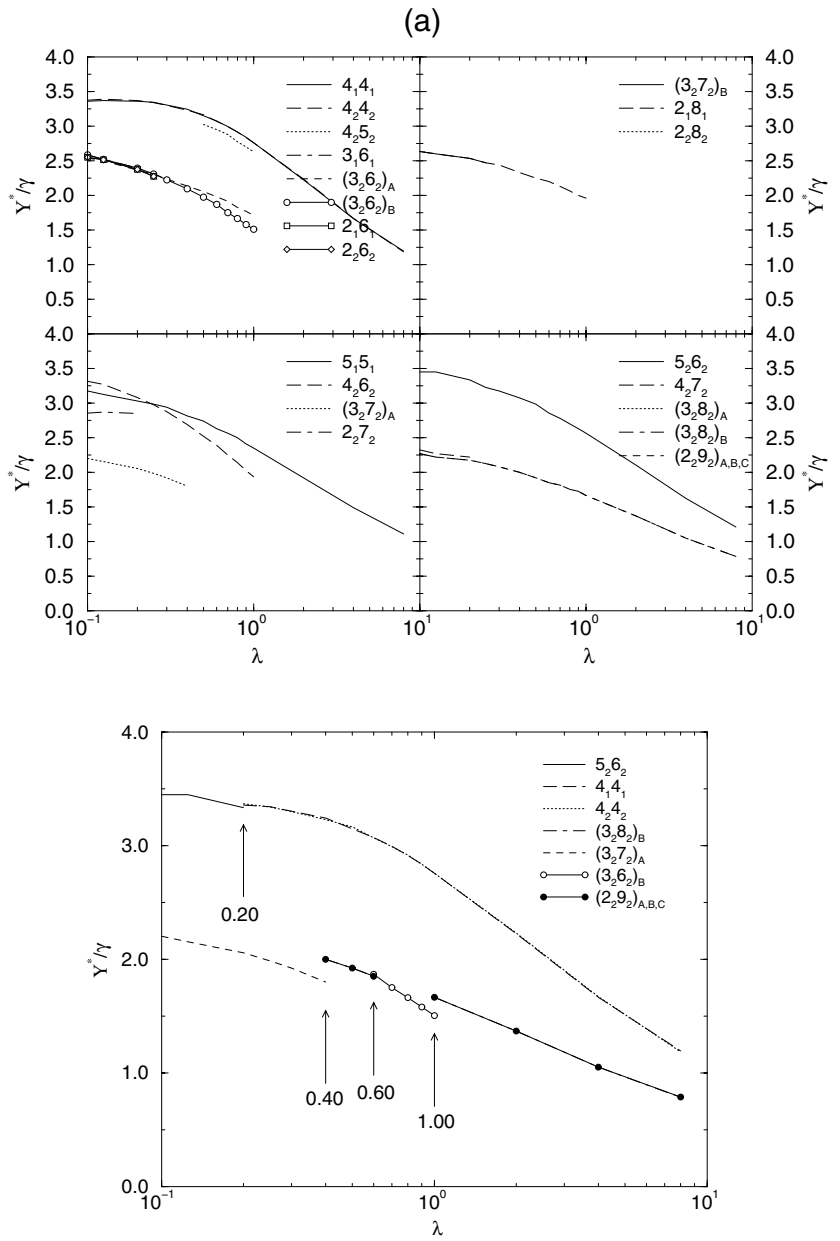

Figure 7. (*a*) Y^*/γ versus λ for all clusters, grouped as in figure 2. (*b*) Smallest (lower set of curves) and largest (upper set of curves) Y^*/γ in each range of λ; the curves for clusters 4_14_1 and 4_24_2, and $(3_28_2)_B$ and $(2_29_2)_{A,B,C}$, are nearly coincident. Note the log-lin scale.

To solve the cluster we first impose angles of 120° between films meeting at vertices, leading to equations of the form

$$\alpha_{12} + \theta_1 + \theta_2 = 120^\circ, \tag{A.2}$$

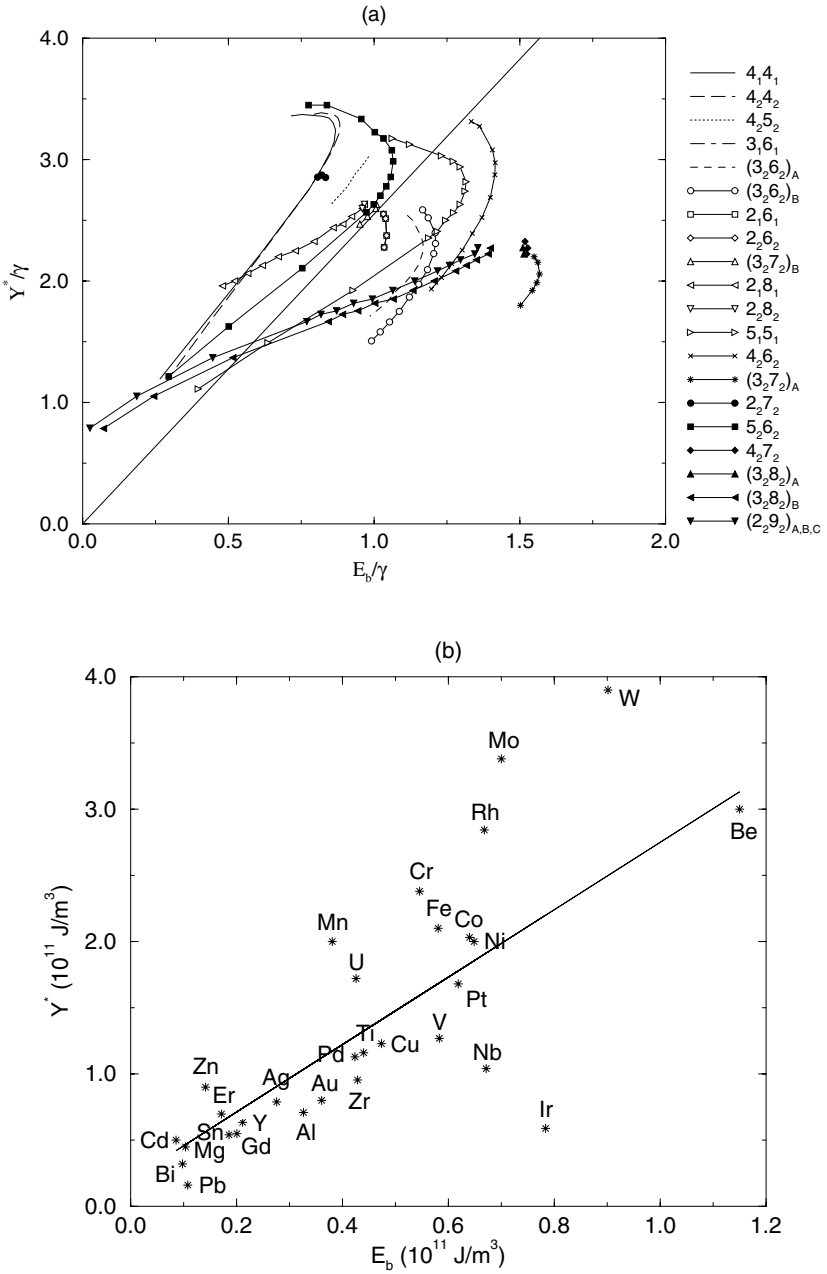

Figure 8. (*a*) Plot of Y^*/γ versus binding energy per unit area E_b/γ for all clusters and for all λ. The straight solid line has the same slope as in part (*b*) below. (*b*) Y^* versus binding energy E_b per unit volume for 30 different metals as labelled (from [11]). The straight line is a linear fit excluding the data point for tungsten; its slope is ≈2.55.

where α_{12} is the angle between two L_i segments with subtended angles $2\theta_1$ and $2\theta_2$. We also impose the balance of pressures, i.e. zero sum of curvatures at each vertex:

$$\sum_i \frac{1}{R_i} = 0. \tag{A.3}$$

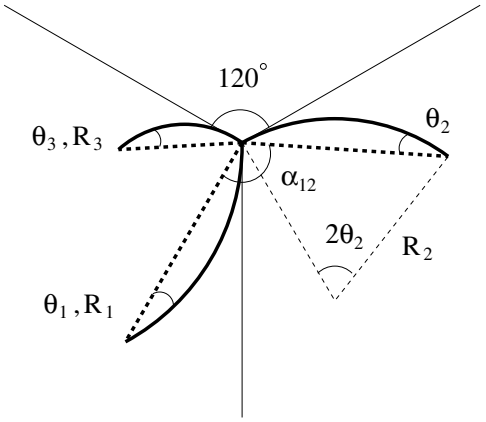

Figure 9. Three films (thick solid curves), each of radius R_i and subtended angle $2\theta_i$, meeting at 120° at a vertex. Their chords (thick dashed lines) meet at angles α_{ik}.

Finally, we write down the equations for the areas of the bubbles in terms of L_i, α_i and θ_i. The number of variables exceeds the number of equations by one. The free variable is chosen to be t, the length along the chain per pair of bubbles. An equation is also derived for the perimeter as a function of the same variables, L_i, α_i and θ_i. This was minimized to find t^* and P^* for a given λ, using the routine DONLP2 [13]. Alternatively, the minimum can be obtained directly from equation (2). To find the full functional dependence $P(\lambda, t)$, we fixed λ and solved the set of equations (A.1)–(A.3) at discrete points in the allowed ranges of t (spacing $\Delta t = 0.01$) for each cluster, using MINPACK routine HYBRD [14]. From these curves Y^* was then calculated by numerical differentiation: three-, five- and 11-point centred-differences formulae, namely

$$\left.\frac{\mathrm{d}^2P}{\mathrm{d}t^2}\right|_{t=t_i} \approx \begin{cases} \dfrac{1}{(\Delta t)^2}[P(t_{i+1}) - 2P(t_i) + P(t_{i-1})] & \text{(3-point)} \\ \dfrac{1}{12(\Delta t)^2}[-P(t_{i+2}) + 16P(t_{i+1}) - 30P(t_i) \\ +\,16P(t_{i-1}) - P(t_{i-2})] & \text{(5-point)} \\ \dfrac{1}{2.52\times10^4(\Delta t)^2}[8P(t_{i+5}) - 125P(t_{i+4}) \\ +10^3P(t_{i+3}) \\ -6\times10^3P(t_{i+2}) + 4\times10^4P(t_{i+1}) \\ -73766P(t_i) + 4\times10^4P(t_{i-1}) \\ -6\times10^3P(t_{i-2}) + 10^3P(t_{i-3}) \\ -125P(t_{i-4}) + 8P(t_{i-5})] & \text{(11-point),} \end{cases} \tag{A.4}$$

gave results differing by at most 0.5%; figure 7 shows those for five points.

References

[1] Herdtle T and Aref H 1992 *J. Fluid Mech.* **241** 233
[2] Glazier J A and Weaire D 1992 *J. Phys.: Condens. Matter* **4** 1867
[3] For reviews see, e.g.,
Kraynik A M 1988 *Annu. Rev. Fluid Mech.* **20** 325
Weaire D and Fortes M A 1994 *Adv. Phys.* **43** 685

[4] Aref H and Vainchtein D L 2000 *Phys. Fluids* **12** 23
[5] Graner F, Jiang Y, Janiaud E and Flament C 2001 *Phys. Rev.* E **63** 011402
[6] Vaz M F and Fortes M A 2001 *J. Phys.: Condens. Matter* **13** 1395
[7] Fortes M A and Teixeira P I C 2001 *Eur. Phys. J.* E **6** 255
[8] Plateau J A F 1873 *Statique Expérimentale et Théorique des Liquides Soumis aux Seules Forces Moléculaires* (Paris: Gauthier-Villars)
[9] Weaire D, Cox S J and Graner F 2002 *Eur. Phys. J.* E **7** 123
[10] Fortes M A 2001 *Phys. Fluids* **13** 3542
[11] Binding energies from Kittel C 1986 *Introduction to Solid State Physics* 6th edn (New York: Wiley)
Young's moduli from Cottrell A H 1967 *An Introduction to Metallurgy* (London: Arnold)
John V B 1992 *Introduction to Engineering Materials* 3rd edn (Basingstoke: Macmillan)
Ashby M F and Jones D H 1980 *Engineering Materials* vol 1 (Oxford: Pergamon)
CRC Handbook of Chemistry and Physics 80th edn 1999 (Boca Raton, FL: Chemical Rubber Company)
Periodic Table of the Elements 1979 Atomic weights and densities (Skokie, IL: Sargent-Welch)
[12] Brakke K 1992 *Exp. Math.* **1** 141 See also http://www.susqu.edu/facstaff/b/ brakke/evolver/evolver.html
[13] Spellucci P http://www.netlib.org/opt/donlp2
[14] http://www.netlib.org/minpack/hybrd.f.